PCCP

ROYAL SOCIETY OF CHEMISTRY

PAPER

View Article Online
View Journal | View Issue

Cite this: *Phys. Chem. Chem. Phys.*, 2026, **28**, 4636

Experimentally confirmed ferroelectricity in organic compounds identified by database mining

Maximilian Litterst,[a] Manjunath Balagopalan,[b] Ramon Jannasch,[a] Elin Dypvik Sødahl,[c] Seyedmojtaba Seyedraoufi,[c] Carl Henrik Gørbitz,[b] Kristian Berland,[c] Ola Nilsen *[b] and Martijn Kemerink *[a]

Compared to inorganic ferroelectrics, the breadth of polarization switching mechanisms in organic ferroelectrics is very broad and far from fully characterized or understood. Here, we experimentally investigate the absence or presence of ferroelectric properties in a selection of organic materials that have been identified by a data mining approach using heuristic measures to identify stretchability, aiming to assess the practical potential of this approach. From a set of 66 candidate materials, 4 were selected for detailed analysis. These were investigated structurally using powder X-ray diffraction and electrically, using capacitance–voltage spectroscopy and polarization hysteresis measurements. Despite large differences in stability and background conductivity, all compounds exhibited ferroelectric behavior at room temperature, with relatively large polarization values. Specifically, the ferroelectric properties of one material show a strong dependency on the ambient humidity, whereas another showed a strong coupling between background conductivity and ferroelectric switching. These effects are not yet fully understood and lie beyond the scope of this study. Of the remaining two compounds, one was found to be unstable at room temperature whereas the other displayed multiple polymorphs, complicating reproducibility and limiting their practical potential. Overall, these results confirm the relevance of the data mining prediction scheme and suggest that a significant fraction of the identified but so far untested materials may also be ferroelectric.

Received 6th August 2025,
Accepted 26th January 2026

DOI: 10.1039/d5cp03009a

rsc.li/pccp

Introduction

Ferroelectric materials are widely used in actuators,[1,2] sensors,[3,4] and power generators[5,6] as well as in non-volatile memory devices.[7] Organic ferroelectrics could potentially replace current heavy-metal-based inorganic materials with non-toxic options and enable new applications such as flexible energy generators.[6] Their typically lower stiffness is advantageous in this context,[6] and their potential for self-healing, linked to the non-covalent bonding in their crystal structures adds further appeal.[8] In addition, organic materials are usually easy-processible, lightweight, and highly tunable. For instance, their conductivity can be modified without compromising their ferroelectric properties.[9] Depending on the application, different material properties are advantageous: piezoelectric actuators benefit from stiffness,[10,11] while softer materials, especially in combination with rotational freedom can be more efficient energy harvesters.[12]

Most inorganic ferroelectrics have an ordered lattice in which the change in polarization arises from a shift in the position of an ion.[13] Such displacive ferroelectrics tend to have comparatively high remnant polarization values and relatively low coercive fields, *e.g.* $P_r \approx 15\ \mu C\ cm^{-2}$ and $E_c \approx 2\ V\ \mu m^{-1}$ for lead zirconate titanate, PZT.[13] Organic or hybrid ferroelectrics can have similar switching mechanisms with the displacement of an ion[14,15] or a charged molecule in a mixed stack, in so-called charge transfer ferroelectrics.[16] Proton transfer ferroelectricity, where a proton changes its position within a hydrogen bond, exists for both organic[17] and inorganic materials.[18] These materials can exhibit very high remnant polarizations and small coercive fields. An example of the latter is croconic acid with $P_r \approx 30\ \mu C\ cm^{-2}$ and $E_c \approx 2\ V\ \mu m^{-1}$.[17] Order–disorder ferroelectrics are mostly organic materials in which permanent dipoles are disordered above the Curie temperature and ordered in the low temperature ferro- or piezoelectric phase. The dipoles can be aligned by an electric field that can reorient the dipolar group,[19] the globular molecule[20] or the whole polymer chain.[21] This class of (organic) ferroelectric materials generally has lower remnant polarizations, limited

[a] *Institute for Molecular Systems Engineering and Advanced Materials, Heidelberg University, Im Neuenheimer Feld 225, 69120 Heidelberg, Germany. E-mail: martijn.kemerink@uni-heidelberg.de*
[b] *Department of Chemistry, University of Oslo, Blindern, N-0315 Oslo, Norway. E-mail: ola.nilsen@kjemi.uio.no*
[c] *Department of Mechanical Engineering and Technology Management, Norwegian University of Life Sciences, 1432 Ås, Norway*

by the dipole moment of the molecule, and higher coercive fields. Well-known examples are the ferroelectric polymer polyvinylidene fluoride (PVDF) and its co-polymers with trifluoroethylene (TrFE), with $P_r \approx 6\ \mu C\ cm^{-2}$ and $E_c \approx 100\ V\ \mu m^{-1}$ for the homopolymer.[22]

While the switching mechanisms and kinetics of inorganic ferroelectrics are generally well understood, the same cannot be said for organic ferroelectrics. Even for PVDF, the most studied organic ferroelectric, the details of switching,[21,23] the reason for its negative piezoelectric coefficient,[24] its structural evolution under poling[25] and the role of (un)intentional structural defects[26,27] are still being investigated. To complement in-depth studies of single-component systems like PVDF and its derivatives or BTA,[28,29] an important way forward in gaining a better understanding of the variety of mechanisms underlying the ferroelectric properties of organic ferroelectrics is to expand the catalogue of known organic ferroelectrics. Not only is this important to establish structure–property relationships, which are currently largely lacking for organic ferroelectrics, but also for identifying their performance limits.

To achieve this, the Cambridge Structural Database (CSD) is a useful resource as was already demonstrated over 30 years ago with a study of 186 materials.[30] With the use of today's computing power, it is possible to screen large portions of the 1.2 million entries according to different criteria depending on the class of ferroelectric being searched for. This approach led to the identification of 54 globular[31] and 12 proton-transfer[32] candidate materials. Here, we assess the validity and relevance of this data mining approach by experimentally investigating whether (a subset of) these materials are indeed ferroelectric.

Out of the many ways to prove ferroelectricity, we selected macroscopic electric measurements of the charge (external quantity of the polarization) and the capacitance (external quantity of the permittivity) because they do not rely on high-quality crystals or thin films, which may be hard to obtain and as such are less suited for a screening study and avoid the additional complications associated with microscopic techniques like piezo-force microscopy.[33,34] At the same time, additional care was taken to avoid spurious signals skewing our interpretation.[35,36] Additionally, the predicted lack of inversion symmetry, which is necessary for ferroelectricity, was confirmed by X-ray diffraction (XRD).

The most direct way to prove ferroelectricity is to measure the polarization *versus* electric field, $P(E)$, hysteresis curve. This is done by applying a triangular voltage waveform, measuring the response current of the material and integrating it, to give the corresponding charge. If the measured charges are indeed due to ferroelectric switching, one should obtain a typical ferroelectric hysteresis loop characterized by polarization saturation once most, if not all, of the dipoles are flipped, visible as a flattening of the polarization above the coercive field.[36] Unfortunately, open but non-saturating loops of integrated charge *vs.* applied field can also arise from a leaky dielectric.[36] Waveforms such as the double wave (two up, two down triangular signals) can be used to isolate, to first order, the polarization switching signal from the resistive and capacitive contributions, thus helping to distinguish true ferroelectrics from 'bananas', *i.e.*, false positives.[37]

For further verification of ferroelectricity, the capacitance–voltage, $C(V)$, loop is advantageous as it helps distinguish leaky dielectrics, whose capacitance typically remains constant. In contrast, ferroelectric materials exhibit a field-dependent permittivity, and as the absolute electric field increases, the capacitance peaks at the coercive field. This occurs because switching creates an energetic equivalence between up and down polarization, resulting in more mobile dipoles.[38]

Other possible measurements include the change of piezoelectricity when switching,[39–42] Curie–Weiß behavior ($\chi(T)^{-1} = \alpha_0(T - T_c)$) indicating the appearance of mobile dipoles[43,44] or second harmonic generation (SHG)[45] and X-ray diffraction to show the existence of a non-centrosymmetric unit-cell, which is a prerequisite for ferroelectricity. To avoid false or ambiguous conclusions, multiple measurements should ideally be performed. However, it is not necessary to perform all of the above-mentioned measurements as this is often not experimentally feasible. *E.g.*, a measurable Curie-temperature may not even exist, for instance when it coincides with, or sits beyond a melting or decomposition point.[46]

Here, we use the double wave measurement to obtain a background corrected hysteresis loop and capacitance–voltage loops. Unfortunately, none of the materials showed Curie–Weiß behavior in dielectric spectroscopy, which can be explained by the fact that none of the materials are stable above 150 °C. Since our focus is on providing a general overview and identifying a methodology to assess whether a compound shows signatures of ferroelectricity and might warrant further investigation, rather than on performing a detailed analysis of the individual materials, we also provide explicit information on our experiences of the reproducibility and practicality of the materials, which are important factors for further investigation.

From the various ferroelectric candidate materials predicted in ref. 31 and 32, four compounds were selected: hexamethylenetetramine hydrogen DL-malate (CSD refcode TOZTAF, from here on called **material 1**), hexamethylenetetramine ammonium tetrafluoroborate (HMTAAB, **material 2**), trimethylamine-borane (ZZZVPE02, **material 3**) and 6-hydroxy-4(3*H*)-pyrimidone (UHUMEP01, **material 4**) mainly because of their high predicted polarization values ($>10\ \mu C\ cm^{-2}$ for **material 1–3**), ease of synthesis (**material 3** and **4** are commercially available), availability of the precursors, and their low-toxicity. All molecule structures are depicted in Fig. 1.

Experimental procedures

Cocrystals of hexamethylene tetramine and DL-malic acid, **material 1**, were synthesized by mixing equimolar mixtures of the precursors (99.0% assay, Sigma Aldrich) as described by Chandrasekhar *et al.*[47] The resulting complex was recrystallized in ethanol and used for various characterizations. Hexamethylenetetramine ammonium tetrafluoroborate, **material 2**, was

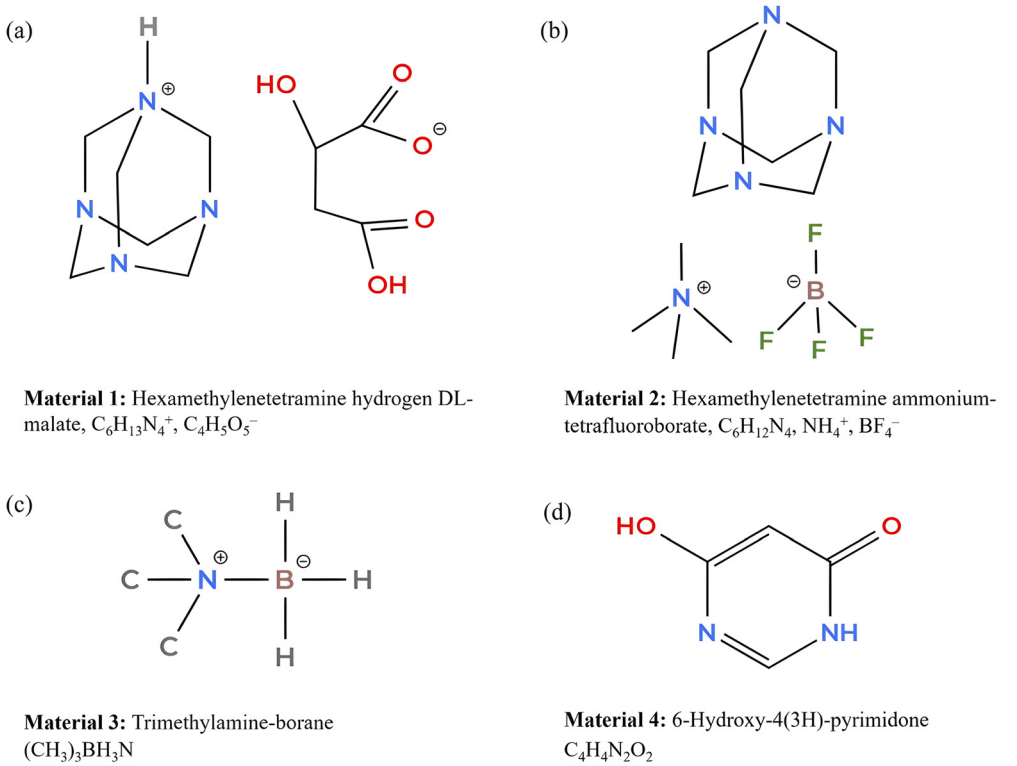

Material 1: Hexamethylenetetramine hydrogen DL-malate, $C_6H_{13}N_4^+$, $C_4H_5O_5^-$

Material 2: Hexamethylenetetramine ammonium-tetrafluoroborate, $C_6H_{12}N_4$, NH_4^+, BF_4^-

Material 3: Trimethylamine-borane $(CH_3)_3BH_3N$

Material 4: 6-Hydroxy-4(3H)-pyrimidone $C_4H_4N_2O_2$

Fig. 1 Molecular structures of **material 1–4** (labeled a–d, respectively) along with their molecular formula.

synthesized by mixing equimolar ratios of hexamethylene tetramine (99.0% assay, Sigma Aldrich) and NH_4BF_4 (99.0% assay, Sigma Aldrich) in water as a solvent. The minimum amount of solvent was used to dissolve the compounds, after which the solution was allowed to evaporate slowly. This synthesis method is reported here for the first time. The compound was recrystallized using ethanol as solvent. Trimethylamineborane, **material 3**, (97% assay) and 6-hydroxy-4(3*H*)-pyrimidone, **material 4**, (98% assay) were directly purchased from Sigma Aldrich and recrystallized from ethanol and water, respectively. Regarding **material 4**, recrystallisation was done under dark conditions, as the compound forms a dimer when recrystallized under sunlight.[48] Fig. 1 summarizes the four compounds studied in this work, along with their CSD reference codes and corresponding molecular formulas.

Powder X-ray diffraction (PXRD) measurements were carried out on a Bruker D2 Phaser diffractometer with a copper source with Cu K_α (λ = 1.541 Å) and molybdenum source with Mo K_α (λ = 0.702 Å) radiation (for **material 4**) in Bragg–Brentano configuration. For PXRD measurements, the compounds were dispersed in ethanol and drop-casted onto a glass substrate. As they were not dissolved this should not have any effect on the crystal structure. All electrical experiments were performed with the material dropcasted on interdigitated electrodes (IDEs). The materials were dissolved with a (low) concentration of 10 mg mL^{-1} in an appropriate solvent (ethanol for **material 1** and **3**, water for **material 2** and **4**). One drop of 5 µL was then dropcasted on the IDE, which resulted in rough, polycrystalline, 1–10 µm thick films, covering approximately half the electrode area. All IDEs had an electrode width and spacing of 5 µm and were made of gold with a chromium adhesion layer. Commercial ED-IDE3-Au IDEs from Micrux (for **material 1–3**) with a circular electrode area (diameter ≈ 3.5 mm), a total electrode length of 0.80 m and an electrode height of 200 nm, as well as homemade IDEs (for **material 4**) with a quadratic electrode area (5 × 5 mm^2) and total electrode length and height of 2.01 m and 35 nm, respectively, were used. Electrical characterization and photos of the empty and filled IDEs are shown in Fig. S6.

While dropcasting films on IDEs allows for simple device fabrication and suffices for our purposes of identifying ferroelectric properties, it is less suited for obtaining absolute values of polarization and permittivity due to the inherent film roughness and the non-linear behavior of ferroelectrics (SI Section S1). Moreover, the polarization change measured only corresponds to the switchable polarization along the axis of the electric field. For a set of randomly (*i.e.*, isotropic) oriented, unmovable dipoles in 3D, the associated correction factor is 0.5; other polarization orientations would correspond to a different value. Non-isotropic orientations and effective correlation factors can arise from polarization rotation due to interaction with the substrate or if the crystal structure allows for multiple polarization directions, as in the case of multiaxial ferroelectrics. However, these factors do not change whether a material class fundamentally exhibits measurable switchable polarization. The question whether a material is ferroelectric can thus still be answered.

All electrical measurements were performed under ambient conditions. $C(V)$ measurements were performed with an Aixacct

TF Analyzer 2000E. The double wave measurements were either performed with the same instrument (**material 1–3**) or with a home-built setup consisting of an input signal supplied by a Tektronix AFG3052C Dual Channel Arbitrary/Function Generator, amplified by a TReK PZD350A high voltage amplifier (**material 4**). In the latter case, the sample response current was measured by a Tektronix TBS 1102B-EDU digital oscilloscope as the voltage dropping over the built-in input resistance of 1 MΩ. The hysteresis curve is then calculated according to the double wave protocol explained in SI Section S2. To compensate for the time-changing capacitance in the $C(V)$ measurement, the data is rescaled according to SI Section S3.

Results and discussion

For context, we start with a brief overview of the structural properties of the investigated compounds. **Material 1** and **2** crystals have ionic molecular structures and belong to the group of hexamine-based compounds. **Material 1** has a monoclinic *Cc* crystal structure at room temperature. Its constituent molecules form several intermolecular hydrogen bonds stabilizing the crystal lattice. The protonated nitrogen makes hydrogen bonds with the carboxylate group of DL maleate. Additionally, the different hydrogen bond lengths for donor and acceptor molecules indicate a possible proton transfer in this system.[47] The calculated polarization is 17.3 μC cm^{-2}.[31] While the theoretical approach screened for globular molecular shapes and hence potential for rotation-driven ferroelectricity, which in principle could be possible but for the specific geometry, it would require the rotation of both molecules to achieve full unit cell inversion. The structure could, however, also be inverted with the rotation of the DL-malic acid and a proton transfer or two proton transfers could yield a not perfectly mirrored state. However, elucidation of the switching mechanism of **material 1** or any of the other compounds investigated herein is beyond the scope of the current work.

Material 2 has a polar hexagonal $P6_3mc$ space group with a perovskite-like structure[49] and no hydrogen bonds. Its polarization is predicted at 11.6 μC cm^{-2} (ref. 31) and can be inverted with the displacement of the positive with respect to the negative ionic molecules. The only other reported hexamethylene-based supposedly ferroelectric system is the hexamethylenetetramine–bisnopinic acid co-crystal. XRD and SHG on this compound indicate a polar space group, the $P(E)$ curve, however, does not saturate and shows a very small polarization of $P_r \approx 0.22$ μC cm^{-2}, indicating that it either results from incomplete switching or does not reflect ferroelectric behavior at all.[50]

Material 3 has a rhombohedral polar $R3m$ space group[51,52] at room temperature. In the database study,[31] only the low temperature phase of this compound (CSD ref code ZZZVPE02, structure reported at 150 K) has been identified as a potential ferroelectric. However, since the reported polar $R3m$ phase is retained even at room temperature (CSD ref.code ZZZVPE, no atomic coordinates published, thus omitted from the data mining study), we have investigated this compound under ambient conditions. (Trimethylamine)-borane has been reported in the literature as plastic crystal with rotational disorder contributing to its metal-like high ductility, malleability and 3D plasticity.[53] These properties of **material 3** can potentially be utilized in flexible and/or wearable ferroelectric devices. It has also showed SHG, piezoelectricity and pyroelectricity, but there is no clear proof of ferroelectric switching as the $P(E)$ loops did not saturate and the PFM spectra do not conclusively rule out an interpretation in terms of (non-ferroelectric) electrostatics.[54] However, the limited thermal stability of **material 3**, see below, seems to be an issue for both characterization and practical applications. Its polarization is predicted at 17.2 μC cm^{-2} and the structure can be inverted with the rotation of the molecule.[31]

The compound 6-hydroxy-4(3*H*)-pyrimidone, **material 4**, an analogue of the RNA nucleobase uracil (2,4-dihydroxypyrimidine), has two monoclinic polymorphs at room temperature: a *Cc* α-form (CSD refcode UHUMEP01) and a $P2_1$ β-form (CSD refcode UHUMEP).[55] Only the former has been predicted to show ferroelectricity based on a proton transfer mechanism.[32] The fact that it can show different polymorphs, of which only UHUMEP01 exhibits the neutral lactam-lactim tautomerization that enables an interconnected proton transfer path,[55] makes it potentially difficult to reach the desired proton-transfer configuration. Its polarization is predicted at 4.41 μC cm^{-2}.[32]

Fig. 2 shows the experimental PXRD patterns of **material 1**, **2** and **4** along with their simulated patterns calculated from their CSD entries. The recrystallized borane complex **material 3** was found to be volatile at room temperature, preventing structural characterization. For the other three compounds, the diffraction peak positions and relative intensities in the simulated patterns agree well with the experimental data. No additional peaks were observed, confirming successful phase formation and absence of any secondary phases. The phase purity in **material 2** supports the reliability of the newly developed synthesis method. Slight discrepancies in relative peak heights for **material 4** are attributed to a preferred orientation of the material, no new peaks were observed in this case either. The XRD measurements were carried out on samples which were crystallized under nominally the same conditions as the material on the IDEs for the ferroelectric characterization. Consequently, the crystal structure of the coated film is expected to correspond to the XRD patterns presented in Fig. 2.

Material 1

When applying the double wave form to **material 1** (Fig. 3a), a double current peak in response to the first voltage wave is obtained, whereas only a single peak (coinciding with the voltage peak) is present in the second wave. For a ferroelectric material, the first double peak includes, apart from any background currents, the charge that is needed to compensate for the change of polarization. When applying the second pulse, the polarization is already switched, so there is no polarization reversal contribution, hence the first peak disappears. Taking the difference between the responses to the first and second

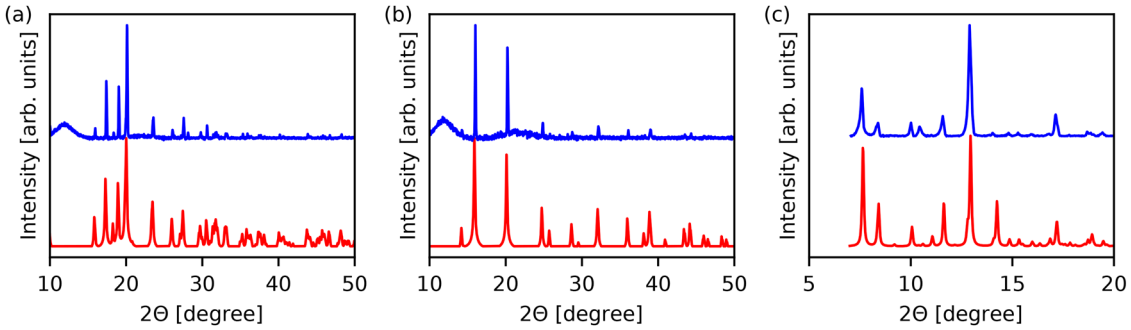

Fig. 2 Measured (blue) powder X-ray diffraction patterns of (a) **material 1**, (b) **material 2** and (c) **material 4** samples along with their simulated patterns (red) obtained from the CSD data base. The hump around $2\theta = 12^\circ$ in (a) and (b) arises from the glass sample holder.

waves and integrating gives the polarization (represented by the charge) hysteresis curves that are shown for different frequencies in (Fig. 3b). For the faster measurements (as well as the curve later shown for **material 2**), there is a sharp edge at 0 V. This is an artefact of the waveform and is explained in more detail in SI Section S2. The charge saturates for each loop, which is necessary for a ferroelectric,[36] and the coercive field sits around 0.35–0.45 V μm^{-1}. The charge associated with ferroelectric switching is determined by crystal geometry and should therefore, contrary to the present data, not depend on the measurement frequency. There might be several reasons for this frequency dependency. It is well known that the coercive field itself is frequency-dependent,[56] thus at higher frequency not all dipoles might be switched. The data however shows a distinct first peak and a saturating hysteresis curve, ruling out this possibility. Alternatively, in many materials there exists a finite ionic conductivity that can give rise to hysteresis.[57] It should predominantly be present in the first pulse of the double wave and should not saturate with increasing field. Hence, ionic currents do give rise to open $P(E)$ loops with increasing 'remnant polarization', but not to any current peaks, as observed here. Hence, ionic contributions to the hysteresis might be present, but can be ruled out as the main source of it. In the evaluation, as detailed in Section S2 of the SI, the current of the second peak is rescaled to match the first peak, ideally compensating for ionic hysteresis in the absolute polarization values. Nevertheless, signs of ionic hysteresis can still be seen in the 250 mHz hysteresis curve (Fig. S9), where the accumulated charge in the hysteresis curve still increases on the decreasing side of the electric field sweep.

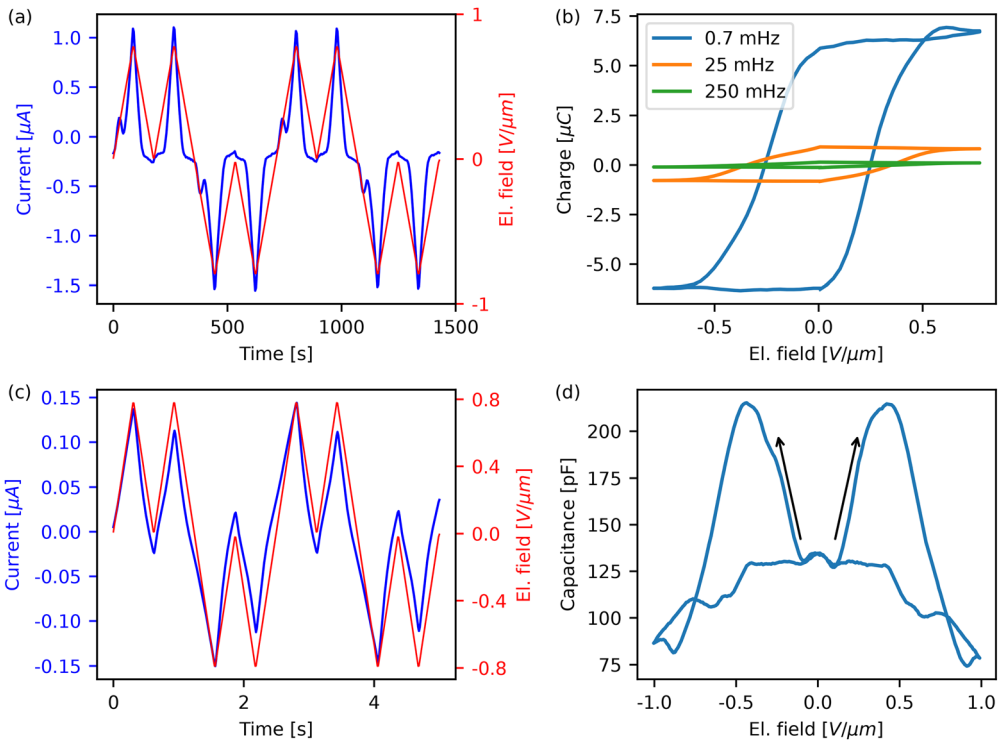

Fig. 3 (a) Double wave signal of **material 1** at ambient conditions with 42%rh; (b) calculated hysteresis curve from (a) and (c) double wave signal of **material 1** at ambient conditions with 19%rh; (d) capacitance–voltage curve of **material 1** with 39%rh.

On top of (minor) ionic contributions, the material also shows significant background conductivity, which is visible as the main peak that is present in both the first and second waves of the DWM and roughly proportional to the driving voltage. The ohmic conductivity in (Fig. 3a) can clearly be attributed to the material, as the empty IDE has negligible leakage, see SI Fig. S4. The evaluation method compensates for the first order background conductivity with the assumption that the background conductivity only depends on the bias.[37] In ferroelectrics, the background conductivity depends on the injection barrier and the bulk conductivity that both may depend on polarization.[58] Specifically, the injection barrier can be altered by a change in surface charge density due to polarization switching[58,59] which can lead to a switch from an injection-limited to a space charge limited regime.[58] The bulk conductivity can also directly depend on the polarization state due to a nonlinear coupling between scattering and polarization.[9,60] In all these cases, the background conductivity below the coercive field cannot properly be compensated for by the DWM. This results in the current peak having contributions from polarization reversal, ionic hysteresis and background conductivity. For lower frequencies, more background conductivity gets integrated, leading to higher calculated charges. Hence, the fastest feasible measurements at 0.25 Hz, result in a charge of 0.11 ± 0.01 μC, which can be converted into an upper limit for the polarization of 54 ± 20 μC cm^{-2} (SI Section S1, S2 and Fig. S9). This finding is consistent with the predicted remnant polarization of 17.3 μC cm^{-2}.[31] Measurements of the $C(V)$-loop (Fig. 3d) show the butterfly shape that is typical for ferroelectrics.[61] There is a broad peak around 0.3–0.5 V μm^{-1} showing good agreement with the coercive field from the hysteresis curve.

Material 1 is quite stable, with samples working for several months, and well-reproducible under the same conditions. There is, however, a strong dependency on the ambient humidity. At low humidity conditions (as can be encountered in winter) all signs of ferroelectric switching disappear (Fig. 3c) and also the background conductivity currents become much smaller, suggesting an interconnectedness.

In summary, **material 1** shows conclusive evidence for ferroelectricity under ambient conditions. The low frequencies that are needed to enable full polarization reversal hint at a more complex mechanism for inversion of the unit cell than mere proton or ion motion, as was anticipated on basis of the complex unit cell. The strong dependence of the ferroelectric and electronic behavior on humidity might actually inspire further investigation of, *e.g.*, the detailed switching mechanism and the role of proton transfer therein and is topic of ongoing investigation.

Material 2

The second compound that was tested was **material 2**. The double wave measurement (Fig. 4a) shows a current peak that is only present in the first wave which is a good sign of ferroelectricity, as well as significant background conductivity. Consequently, the hysteresis curve (Fig. 4b) saturates which is a prerequisite for ferroelectricity. The integrated charge at the maximum voltage accumulates to 2.4 μC, which would correspond to an unreasonable saturation polarization of 1200 ± 400 μC cm^{-2}. As for **material 1**, this can be explained by a dependence of the conductivity on polarization, and specifically by the conductivity before switching being increased. For this reason, the integrated charge is the sum of the true polarization charge and the integrated difference in background conductivity current.

After the maximum field, the charge slightly increases to 2.8 μC at zero field. This can be explained by incomplete background conductivity compensation as the current of the first peak is always slightly above the peak from the second peak (Fig. S11) in combination with a minor contribution from ionic hysteresis. The coercive field is ≈0.4 V μm^{-1}. The $C(V)$-loop (Fig. 4b) shows the characteristic butterfly shape with a peak at ≈0.4 ± 0.5 V μm^{-1}, indicating good agreement between the two measurements for the coercive fields and confirming the ferroelectric nature of the compound.

In summary, there is conclusive evidence that **material 2** is ferroelectric. While the ferroelectric properties are not remarkable, the potential coupling to background conductivity are yet to be understood and a topic of ongoing investigation.[9,59,62] Due to its fast degradation, the material does not seem very promising for applications.

Material 3

Measurements using the known piezo- and pyroelectric **material 3** proved more challenging than those with the previously mentioned materials. These difficulties arise from the

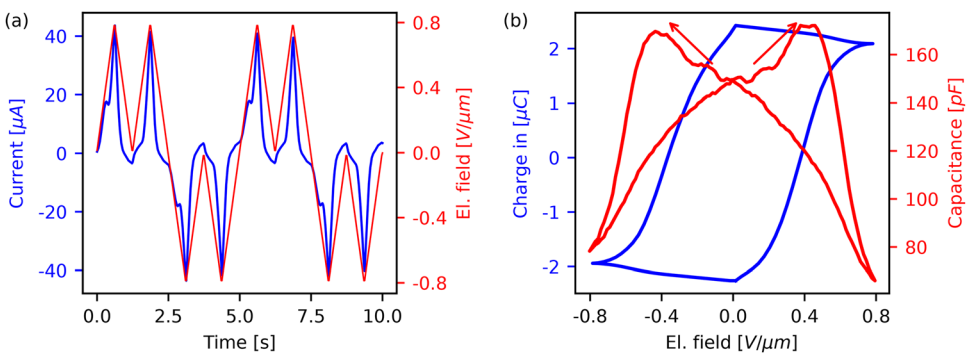

Fig. 4 (a) Double wave signal of **material 2**, fabricated with water as solvent; (b) blue: hysteresis curve calculated from (a); red: $C(V)$ curve.

material's tendency to sublimate quickly at ambient conditions. For this reason, all experiments had to be performed immediately after device fabrication. The double wave measurements of one device (Fig. 5a) depict very sharp current peaks that are only present in the first wave. The presence in the first wave and the absence in the second is usually good evidence for ferroelectricity. In this case, the peaks are, however, unusually narrow and have varying heights; they do, however, always sit at a well-defined (possible) coercive field of 13.3 ± 0.5 V μm^{-1}. Combined, this leads to the strange shape of the hysteresis curve in Fig. 5b where the apparent change of polarization is different for both directions and the change in polarization is very steep. In principle, the sharpness might be indicative of fast switching in a low-disorder, *i.e.* close to intrinsic, sample. However, due to the problematic (in)stability of the material, discussed further below, it was not possible to investigate this further.

One further noteworthy feature of the DWM signals in Fig. 5a is the fact that the conductivity after the polarization reversal event in the first wave is increased. This is opposite to what occurs in **material 2** and, to a lesser degree, in TOZFAF. In principle, such behavior could result from the modulation of a charge injection barrier by the orientation of the interfacial dipoles, giving rise to easier charge injection when polarization and field are parallel.[9,59] The increased current is not compensated for by the evaluation method,[37] leading to the linear increase of charge in the $P(E)$-loop above the (possible) coercive field. What speaks against this interpretation is the conductivity in the second wave of the DWM being at the same level as that in the first wave prior to the supposed switching. In an injection barrier modulation scenario, the interfacial dipoles should, when still aligned, continue to allow an enhanced injection. In absence of secondary peaks indicating full polarization loss between the two waves, one might tentatively attribute the odd conductivity behavior to the interfacial, but not the bulk polarization being quickly lost.

The charge at maximum voltage is 3.5 × 10^{-4} μC. As the material sublimates very quickly, it is difficult to determine the exact film structure. The, in this case unreasonable, assumption of a thick (>500 nm), continuous film would result in a very low polarization (0.09 μC cm^{-2}) compared to the predicted value (17.2 μC cm^{-2}).[31] $C(V)$-Measurements of the same sample (Fig. S14a) did not show the typical butterfly shape. Measurements of other samples occasionally showed peaks in the first wave (Fig. S14b), but any reliable appearance could not be achieved. This poor reproducibility can be attributed to the quick sublimation of the material, which makes every experiment difficult.

In summary, the results presented here are by themselves inconclusive. While the appearance of peaks of DWM generally suggests ferroelectricity, the unusual peak-shape and the absence of butterfly-like $C(V)$-loop casts doubt on this interpretation. Nevertheless, as the material has already been shown to exhibit SHG, piezoelectricity and pyroelectricity,[54] we believe that the here shown measurements are sufficient to at least suggest a field-induced reversal of the (previously shown) dipolar inversion asymmetry in the material, that is, ferroelectricity. Given the challenges associated with handling this material, future efforts should focus on identifying more suitable conditions for working with it.

Material 4

The last substance that was investigated is the proton-transfer **material 4**. The double wave measurement (Fig. 6a) reproducibly show additional current shoulders in the first voltage wave that do not show up in the second. This results in a saturating hysteresis curve (Fig. 6b) with a coercive field of 8 V μm^{-1} and a remnant charge of 2.1 × 10^{-2} μC resulting in a remnant polarization of 4.2 ± 1.4 μC cm^{-2} for a DWM cycle frequency of 2 Hz. A possible effect of conductivity switching is suppressed by the comparably high measurement speed. On basis of the calculated energy barrier for proton transfer, the coercive field for a 5 Hz (equivalent to 2.5 Hz in DWM) measurement was estimated to be around 1.3 V μm^{-1}.[32] It is worth underlining that predictions of proton-transfer barrier are highly method dependent.[63] This means that the measured coercive field is similar to but higher than expected. The estimated remnant polarization from the hysteresis loop is surprisingly close to the predicted value of 4.41 μC cm^{-2},[32] given that many of the used parameters are only rough estimates.

The $C(V)$-loop (Fig. 6c) shows the typical butterfly-shape with a peak at 0.6 V μm^{-1}. The difference between the different

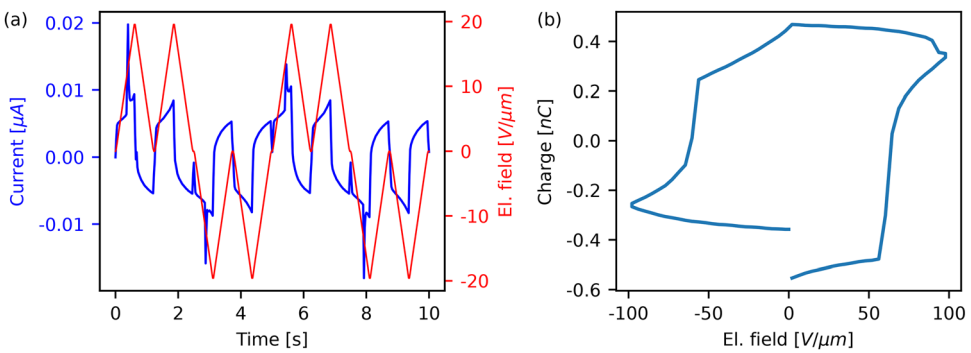

Fig. 5 (a) Double wave signal of **material 3** at ambient conditions, (b) the calculated hysteresis curve from (a). The current peaks after each 2nd wave are due to the short plateau in the driving voltage signal and do not reflect any form of switching or shorting.

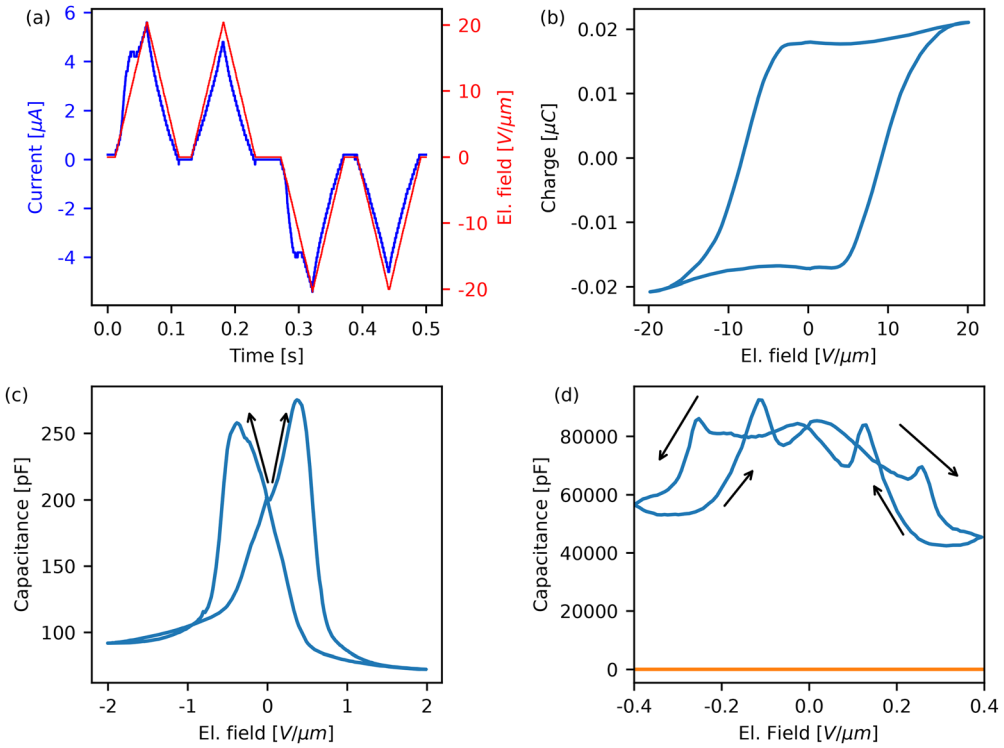

Fig. 6 (a) Double wave signal of **material 4** at ambient conditions, (b) the calculated hysteresis curve from (a) and (c) representative capacitance–voltage curve of **material 4** at ambient conditions (d) capacitance–voltage curves of two different selected samples from the same batch as (c).

coercive fields can be explained by the measurement frequency, which is 2 Hz for the double wave measurement and 0.004 Hz for the $C(V)$-measurement.

The material is known to have multiple polymorphs (including a dimerized form) and tautomers,[48,55] of which only one polymorph was predicted to be ferroelectric. The dimer is easily identifiable as it forms long needles.[48] An optical microscopy image (Fig. S6c) of this sample shows some needles, indicating that the dimeric form is also present in small amounts. As the dimer has no transferable proton on the oxygen in the molecule, it is expected to be electrically inactive and its presence should therefore not influence the results. This multitude of different states is, amongst others, reflected in a minority of samples being electrically inactive as indicated by the orange curve in Fig. 6d. In this particular case, the material only consisted of needles (Fig. S6d), indicating the dimeric state and confirming that the dimeric form is electrically inactive. In stark contrast, another sample showed a very high permittivity and a capacitance peak at $\sim$0.3 V μm^{-1} when increasing the electric field and another peak at a lower field of $\sim$0.1 V μm^{-1} when decreasing the field, as shown by the blue line in Fig. 6d. This behavior resembles the $C(V)$-loop of an anti-ferroelectric.[64] The corresponding double wave measurement (Fig. S16a), however, never showed the currents that are associated with an anti-ferroelectric,[37] so the nature of this phenomenon remains somewhat unclear. Optical microscopy (Fig. S6e) showed that the dimeric form is not present in this sample. As the other polymorph was never observed in XRD experiments, we do not expect this polymorph but rather a different tautomer to be present in this sample, as they cannot be distinguished with XRD.

In summary, we are convinced that at least one of the states of **material 4** is a well-behaved ferroelectric, while potentially one or more of the other states might also show interesting or at least different behavior. As expected, the dimeric form seems to be electrically inactive. At the same time, the limited reproducibility makes systematic work on this material challenging. To properly understand its ferroelectric properties, it is first necessary to establish reliable methods for achieving the desired state. However, this lies beyond the scope of the present exploratory study.

Conclusion and outlook

In this study, we experimentally investigated four materials that were predicted to be ferroelectric in a database mining approach. The dual aim was to assess the effectiveness of this method for discovering new organic ferroelectric compounds with interesting properties and to improve our understanding of structure–property-relationships in such systems. For three materials (**1**, **2** and **4**), the double wave measurement revealed clear polarization switching currents that appeared in the first voltage pulse, but not the second, resulting in saturated hysteresis loops. The corresponding capacitance–voltage-curves exhibited the characteristic butterfly shape, which, together with the polarization hysteresis behavior, provides strong evidence for ferroelectricity. The double wave measurement of **material 3** showed a strong, unusually sharp current peak in the

first pulse, which could indicate ferroelectricity switching. However, this result could not be reproduced, and the $C(V)$-loop lacks the expected butterfly-shape, rendering the findings inconclusive. Based on this success rate, it can be inferred that there are likely several dozen yet unconfirmed ferroelectric materials among the candidates proposed by the database mining, thereby validating the effectiveness of the specific database mining approach.

While there is only one possible switching mechanism for **material 2** and **4**, the mechanism for **material 1** remains unclear due to the presence of multiple potential pathways. Further investigation, particularly through humidity-dependent studies, could help clarify the switching behavior and contribute to a deeper understanding of switching phenomena in more complex ferroelectric co-crystals. Insights gained from such studies could, in turn, enhance the screening process by incorporating not only polarization values, but also the feasibility and nature of the switching pathway. Furthermore, understanding the interplay between humidity and ferroelectricity in **material 1** might give new insights on the role of water as a nucleation center or the influence of humidity on proton-transfer ferroelectrics. **Material 2** showed strong conductivity-ferroelectricity coupling. Having shown that both of these hexamine-based materials are ferroelectric and show additional, previously unknown coupling between ferroelectricity and humidity or background conductivity, a logical follow up would be to investigate comparable materials. The screening study suggested two other hexamine-based candidate materials. While 1,3,5-triaza-9-phospha-adamantane (TAZPAD) is a single-compound material with small predicted polarization and therefore not really comparable to **material 1** and **2**, it also tends to sublimate at room temperature which drastically reduces its usability. On the other hand, 1,3,5,7-tetra-aza-adamantan-1-ium bromide (BOHNUH01) is also an ionic co-crystal with comparable predicted polarization and therefore promising to investigate for ferroelectricity and coupling between ferroelectricity, humidity and conductivity.

Our study has demonstrated that database mining is a viable path to identify novel organic ferroelectrics. This approach can be expanded with other filter criteria to find different kinds of ferroelectric materials. Two examples of well-known molecular ferroelectrics that were, due to the chosen criteria, not 'discovered' in the database mining are the benzene-1,3,5-trisamide (BTA) and polyvinylidene fluoride (PVDF) families of materials; especially for the former it seems possible to identify generalized and transferable detection criteria. In its current shape, the used methodology is, however, limited to materials that are available in the underlying database and to materials which follow the chosen criteria which are usually based on known ferroelectrics. Our results also emphasize the importance of adding additional assessment criteria, such as melting temperature, vapor pressure or in general other decomposition paths. Both cohesion energies from DFT or (possible in combination with) machine learning methods should have strong prospects of providing such predictions. From an experimental point of view, additional pragmatic filters such as simple estimates of vapor pressure or environmental stability can help improve the initial screening.

Database mining, or traditional intuitive trial-and-error approaches, are not the only way to engineer new ferroelectric materials. A key limitation in our assessment was the fact that many of the predicted ferroelectrics from database mining could not easily be acquired. A pragmatic approach, especially suited for theory-experiment collaborations could be to only start from those molecules that are easily available or synthesized and attempt to identify those combinations that would adopt a crystalline packing supporting ferroelectricity. While computationally demanding, crystal structure prediction (CSP) can be used for this purpose.[65] However, with growing computational power and increasingly refined workflows[66,67] and ingratiation of machine learning force fields[68] and similar methods, we can expect such approaches to become more common.

The challenge of identifying switching paths could also greatly benefit from computational approaches, but a first, possible more addressable challenge (since it does not require incorporation of external fields) is to understand phase transition in these compounds, which can benefit from the recent machine learning force fields that can be used in molecular dynamics simulations, as recently done for the HdabcoClO4 ferroelectric molecular crystal.[69] However, understanding complex switching paths, including nucleation effects may also require novel multi-scale approaches, or a combination of combinations of computational and heuristic assessments.

Conflicts of interest

The authors declare no conflicts of interest.

Data availability

The data supporting this article has been included as part of the manuscript and its supplementary information (SI). Supplementary information is available. See DOI: https://doi.org/10.1039/d5cp03009a.

Acknowledgements

Work by MB, KB, SS, EDS, CHG, and ON was supported by the Research Council of Norway as a part of the Young Research Talent project FOX (302362). M. K. thanks the Carl Zeiss Foundation for financial support.

References

1 H. Jin, X. Gao, K. Ren, J. Liu, L. Qiao, M. Liu, W. Chen, Y. He, S. Dong, Z. Xu and F. Li, Review on Piezoelectric Actuators Based on High-Performance Piezoelectric Materials, *IEEE Trans. Ultrason. Eng.*, 2022, **69**, 3057–3069.
2 X. Gao, J. Yang, J. Wu, X. Xin, Z. Li, X. Yuan, X. Shen, S. Dong, X. Gao, J. Yang, J. Wu, X. Xin, Z. Li, X. Yuan, X. Shen

and S. Dong, Piezoelectric Actuators and Motors: Materials, Designs, and Applications, *Adv. Mater. Technol.*, 2020, **5**, 1900716.

3 J. F. Tressler, S. Alkoy and R. E. Newnham, Piezoelectric Sensors and Sensor Materials, *J. Electroceram.*, 1998, **2**, 257–272.

4 M. Sawane and M. Prasad, MEMS piezoelectric sensor for self-powered devices: a review, *Mater. Sci. Semicond. Process.*, 2023, **158**, 107324.

5 N. Sezer and M. Koç, A comprehensive review on the state-of-the-art of piezoelectric energy harvesting, *Nano Energy*, 2021, **80**, 105567.

6 D. B. Deutz, J. A. Pascoe, B. Schelen, S. Van Der Zwaag, D. M. De Leeuw and P. Groen, Analysis and experimental validation of the figure of merit for piezoelectric energy harvesters, *Mater. Horiz.*, 2018, **5**, 444–453.

7 T. Mikolajick, U. Schroeder and S. Slesazeck, The Past, the Present, and the Future of Ferroelectric Memories, *IEEE Trans. Electron Devices*, 2020, **67**, 1434–1443.

8 S. Bhunia, S. Chandel, S. K. Karan, S. Dey, A. Tiwari, S. Das, N. Kumar, R. Chowdhury, S. Mondal, I. Ghosh, A. Mondal, B. B. Khatua, N. Ghosh and C. Malla Reddy, Autonomous self-repair in piezoelectric molecular crystals, *Science*, 2021, **373**, 321–327.

9 N. M. Casellas, I. Urbanaviciute, T. D. Cornelissen, J. A. Berrocal, T. Torres, M. Kemerink and M. García-Iglesias, Resistive switching in an organic supramolecular semiconducting ferroelectric, *Chem. Commun.*, 2019, **55**, 8828–8831.

10 F. Giraud and C. Giraud-Audine, *Piezoelectric Actuators: Vector Control Method: Basic, Modeling and Mechatronic Design of Ultrasonic Devices*, Elsevier, 2019.

11 J. Walker, E. D. Sødahl, S. Scherrer, K. Marshall, D. Chernyshov, K. Berland and T. Rojac, Electromechanical properties of uniaxial polar ionic plastic crystal $[(C_2H_5)_4N][FeBrCl_3]$, *JPhys: Energy*, 2024, **6**, 025026.

12 E. D. Sødahl, J. Walker and K. Berland, Piezoelectric Response of Plastic Ionic Molecular Crystals: Role of Molecular Rotation, *Cryst. Growth Des.*, 2023, **23**, 729–740.

13 P. K. Panda and B. Sahoo, PZT to Lead Free Piezo Ceramics: A Review, *Ferroelectrics*, 2015, **474**, 128–143.

14 Z. Sun, A. Zeb, S. Liu, C. Ji, T. Khan, L. Li, M. Hong, J. Luo, D. Sun, C. Ji, D. Li, M. Hong, J. Luo, A. Zeb, S. Liu and T. Khan, Exploring a Lead-free Semiconducting Hybrid Ferroelectric with a Zero-Dimensional Perovskite-like Structure, *Angew. Chem.*, 2016, **128**, 12033–12037.

15 Y. Hu, L. You, B. Xu, T. Li, S. A. Morris, Y. Li, Y. Zhang, X. Wang, P. S. Lee, H. J. Fan and J. Wang, Ferroelastic-switching-driven large shear strain and piezoelectricity in a hybrid ferroelectric, *Nat. Mater.*, 2021, **20**, 612–617.

16 F. Kagawa, S. Horiuchi, M. Tokunaga, J. Fujioka and Y. Tokura, Ferroelectricity in a one-dimensional organic quantum magnet, *Nat. Phys.*, 2010, **6**, 169–172.

17 S. Horiuchi, K. Kobayashi, R. Kumai and S. Ishibashi, Proton tautomerism for strong polarization switching, *Nat. Commun.*, 2017, **8**, 1–9.

18 R. S. Pease and G. E. Bacon, Ferroelectric Structure of Potassium Dihydrogen Phosphate, *Nature*, 1954, **173**, 443–444.

19 A. V. Gorbunov, T. Putzeys, I. Urbanavičiute, R. A. J. Janssen, M. Wübbenhorst, R. P. Sijbesma and M. Kemerink, True ferroelectric switching in thin films of trialkylbenzene-1,3,5-tricarboxamide (BTA), *Phys. Chem. Chem. Phys.*, 2016, **18**, 23663–23672.

20 J. Harada, T. Shimojo, H. Oyamaguchi, H. Hasegawa, Y. Takahashi, K. Satomi, Y. Suzuki, J. Kawamata and T. Inabe, Directionally tunable and mechanically deformable ferroelectric crystals from rotating polar globular ionic molecules, *Nat. Chem.*, 2016, **8**, 946–952.

21 W. J. Hu, D. M. Juo, L. You, J. Wang, Y. C. Chen, Y. H. Chu and T. Wu, Universal Ferroelectric Switching Dynamics of Vinylidene Fluoride-trifluoroethylene Copolymer Films, *Sci. Rep.*, 2014, **4**, 1–8.

22 B. Dickens, E. Balizer, A. S. DeReggi and S. C. Roth, Hysteresis measurements of remanent polarization and coercive field in polymers, *J. Appl. Phys.*, 1992, **72**, 4258–4264.

23 M. S. Ravisankar and R. B. Gangineni, Study of relaxation kinetics in PVDF interconnected nanodots using piezo force microscopy, *J. Mater. Sci.: Mater. Electron.*, 2023, **34**, 1–9.

24 Y. Liu, Q. Wang, Y. Liu and Q. Wang, Ferroelectric Polymers Exhibiting Negative Longitudinal Piezoelectric Coefficient: Progress and Prospects, *Adv. Sci.*, 2020, **7**, 1902468.

25 C. Revenant, S. Toinet, E. Lawrence Bright and M. Benwadih, The Longitudinal and Transverse Piezoelectric Effects of the Ferroelectric Polymer P(VDF-TrFE), *Macromol. Mater. Eng.*, 2025, 2400420.

26 X. Wang, B. Qiao, S. Tan, W. Zhu and Z. Zhang, Tuning the ferroelectric phase transition of PVDF by uniaxially stretching crosslinked PVDF films with CF[double bond, length as m-dash]CH bonds, *J. Mater. Chem. C*, 2020, **8**, 11426–11440.

27 H. Gong, X. Wang, M. Sun, Y. Zhang, Q. Ji and Z. Zhang, Tuning the Ferroelectric Phase Transition of P(VDF-TrFE) through a Simple Approach of Modification by Introducing Double Bonds, *ACS Omega*, 2022, **7**, 42949–42959.

28 I. Urbanaviciute, X. Meng, T. D. Cornelissen, A. V. Gorbunov, S. Bhattacharjee, R. P. Sijbesma and M. Kemerink, Tuning the Ferroelectric Properties of Trialkylbenzene-1,3,5-tricarboxamide (BTA), *Adv. Electron. Mater.*, 2017, **3**, 1600530.

29 I. Urbanaviciute, S. Bhattacharjee, M. Biler, J. A. M. Lugger, T. D. Cornelissen, P. Norman, M. Linares, R. P. Sijbesma and M. Kemerink, Suppressing depolarization by tail substitution in an organic supramolecular ferroelectric, *Phys. Chem. Chem. Phys.*, 2019, **21**, 2069–2079.

30 Z. Zikmund, P. Vaněk, M. Havránková, B. Březina, M. člermák, M. Vásša, P. Vanek, M. Havrankova, B. Brezina, M. Cermak and M. Vasa, Search for new molecular organic ferroelectrics, *Ferroelectrics*, 1994, **158**, 223–228.

31 E. Dypvik Sødahl, S. Seyedraoufi, C. H. Görbitz and K. Berland, Ferroelectric Crystals of Globular Molecules: Cambridge Structural Database Mining and Computational Assessment, *Cryst. Growth Des.*, 2023, **23**, 8607–8619.

32 S. Seyedraoufi, E. D. Sødahl, C. H. Görbitz and K. Berland, Database mining and first-principles assessment of organic proton-transfer ferroelectrics, *Phys. Rev. Mater.*, 2024, **8**, 054413.
33 D. Seol, B. Kim and Y. Kim, Non-piezoelectric effects in piezoresponse force microscopy, *Curr. Appl. Phys.*, 2017, **17**, 661–674.
34 N. Balke, P. Maksymovych, S. Jesse, A. Herklotz, A. Tselev, C.-B. Eom, I. I. Kravchenko, P. Yu and S. V. Kalinin, Differentiating Ferroelectric and Nonferroelectric Electromechanical Effects with Scanning Probe Microscopy, *ACS Nano*, 2015, **9**, 6484–6492.
35 M. Litterst, A. A. Butkevich and M. Kemerink, Inconclusive proof of ferroelectricity in peptide-VDF ribbons, *Nature*, 2025, **644**, E1–E3.
36 J. F. Scott, Ferroelectrics go bananas, *J. Phys.: Condens. Matter*, 2008, **20**, 9–11.
37 M. Fukunaga and Y. Noda, New Technique for Measuring Ferroelectric and Antiferroelectric Hysteresis Loops, *J. Phys. Soc. Jpn.*, 2008, **77**, 064706.
38 D. Damjanovic, Ferroelectric, dielectric and piezoelectric properties of ferroelectric thin films and ceramics, *Rep. Prog. Phys.*, 1998, **61**, 1267.
39 N. Balke, P. Maksymovych, S. Jesse, A. Herklotz, A. Tselev, C. B. Eom, I. I. Kravchenko, P. Yu and S. V. Kalinin, Differentiating Ferroelectric and Nonferroelectric Electromechanical Effects with Scanning Probe Microscopy, *ACS Nano*, 2015, **9**, 6484–6492.
40 B. Kim, D. Seol, S. Lee, H. N. Lee and Y. Kim, Ferroelectric-like hysteresis loop originated from non-ferroelectric effects, *Appl. Phys. Lett.*, 2016, **109**, 102901.
41 D. Seol, B. Kim and Y. Kim, Non-piezoelectric effects in piezoresponse force microscopy, *Curr. Appl. Phys.*, 2017, **17**, 661–674.
42 I. Urbanaviciute, *et al.*, Negative piezoelectric effect in an organic supramolecular ferroelectric, *Mater. Horiz.*, 2019, **6**, 1688–1698.
43 P. Chandra and P. B. Littlewood, A Landau Primer for Ferroelectrics, *Top. Appl. Phys.*, 2007, **105**, 69–116.
44 A. V. Gorbunov, T. Putzeys, I. Urbanavičiute, R. A. J. Janssen, M. Wübbenhorst, R. P. Sijbesma and M. Kemerink, True ferroelectric switching in thin films of trialkylbenzene-1,3,5-tricarboxamide (BTA), *Phys. Chem. Chem. Phys.*, 2016, **18**, 23663–23672.
45 R. W. Boyd, *Nonlinear Opt.*, 2020, 1–64.
46 A. J. Lovinger, Ferroelectric Polymers, *Science*, 1983, **220**, 1115–1121.
47 S. Chandrasekhar and S. Mukherjee, Salts of hexamethylenetetramine with organic acids: enhanced anomeric interactions with a lowering of molecular symmetry revealed by crystal structures, *J. Mol. Struct.*, 2015, **1082**, 188–194.
48 A. Katrusiak and A. Katrusiak, Crystal-stabilisation of an elusive 4,6-pyrimidinedione dimer, *Tetrahedron Lett.*, 2007, **48**, 1935–1938.
49 E. Fluck and W. Schwarz, NH_4BF_4 $(CH_2)N_4$, *Z. Anorg. Allg. Chem.*, 1978, **444**, 121–124.
50 C. S. Yang, Y. H. Tan, C. F. Wang, S. P. Chen, B. Wang, H. R. Wen and Y. Z. Tang, Exceptional second harmonic generation responses, switchable dielectric behaviours, and ferroelectric property in an adduct of hexamethylene-tetramine·bisnopinic acid, *Chem. Phys.*, 2018, **502**, 66–71.
51 S. Aldridge, A. J. Downs, C. Y. Tang, S. Parsons, M. C. Clarke, R. D. L. Johnstone, H. E. Robertson, D. W. H. Rankin and D. A. Wann, Structures and aggregation of the methylamine-borane molecules, $Me_nH_{3-n}N\,BH_3$ (n = 1–3), studied by X-ray diffraction, gas-phase electron diffraction, and quantum chemical calculations, *J. Am. Chem. Soc.*, 2009, **131**, 2231–2243.
52 S. Geller, R. E. Hughes and J. L. Hoard, Note on the crystalline structure of trimethylamine–borine, $(H_3C)_3N$–BH_3, *Acta Crystallogr.*, 1951, **4**, 380.
53 A. Mondal, B. Bhattacharya, S. Das, S. Bhunia, R. Chowdhury, S. Dey and C. M. Reddy, Metal-like Ductility in Organic Plastic Crystals: Role of Molecular Shape and Dihydrogen Bonding Interactions in Aminoboranes, *Angew. Chem., Int. Ed.*, 2020, **59**, 10971–10980.
54 Y. Zhang, M. A. Hopkins, D. J. Liptrot, H. Khanbareh, P. Groen, X. Zhou, D. Zhang, Y. Bao, K. Zhou, C. R. Bowen and D. R. Carbery, Harnessing Plasticity in an Amine-Borane as a Piezoelectric and Pyroelectric Flexible Film, *Angew. Chem., Int. Ed.*, 2020, **59**, 7808–7812.
55 A. Katrusiak and A. Katrusiak, Ionic disparity of identical molecules in polymorphs, *Org. Lett.*, 2003, **5**, 1903–1905.
56 L. Jin, F. Li and S. Zhang, Decoding the Fingerprint of Ferroelectric Loops: Comprehension of the Material Properties and Structures, *J. Am. Ceram. Soc.*, 2014, **97**, 1–27.
57 D. A. Jacobs, Y. Wu, H. Shen, C. Barugkin, F. J. Beck, T. P. White, K. Weber and K. R. Catchpole, Hysteresis phenomena in perovskite solar cells: the many and varied effects of ionic accumulation, *Phys. Chem. Chem. Phys.*, 2017, **19**, 3094–3103.
58 P. W. M. Blom, R. M. Wolf, J. F. M. Cillessen and M. P. C. M. Krijn, Ferroelectric Schottky diode, *Phys. Rev. Lett.*, 1994, **73**, 2107–2110.
59 A. V. Gorbunov, M. G. Iglesias, J. Guilleme, T. D. Cornelissen, W. S. C. Roelofs, T. Torres, D. González-Rodríguez, E. W. Meijer and M. Kemerink, Ferroelectric self-assembled molecular materials showing both rectifying and switchable conductivity, *Sci. Adv.*, 2017, **3**, e1701017.
60 T. Johann, W. Xie, S. Roosta, M. Elstner and M. Kemerink, Theory for nonlinear conductivity switching in semiconducting organic ferroelectrics, *Phys. Chem. Chem. Phys.*, 2024, **26**, 18837–18846.
61 D. Bolten, U. Böttger and R. Waser, Reversible and irreversible polarization processes in ferroelectric ceramics and thin films, *J. Appl. Phys.*, 2003, **93**, 1735–1742.
62 H. Mager, M. Litterst, S. Klubertz, S. V. Haridas, O. Shyshov, M. von Delius and M. Kemerink, A supramolecular ferroelectric with two sublattices and polarization dependent conductivity, *arXiv*, 2025, preprint, arXiv:2507.11309, DOI: 10.48550/arXiv.2507.11309.

63 S. Seyedraoufi and K. Berland, Improved proton-transfer barriers with van der Waals density functionals: role of repulsive non-local correlation, *J. Chem. Phys.*, 2022, **156**, 244106.
64 F. Zhuo, H. Qiao, J. Zhu, S. Wang, Y. Bai, X. Mao and H. H. Wu, Perspective on antiferroelectrics for energy storage and conversion applications, *Chin. Chem. Lett.*, 2021, **32**, 2097–2107.
65 S. Seyedraoufi, G. M. Day and K. Berland, Design of novel organic proton-transfer acid–base (anti-)ferroelectric salts with crystal structure prediction, *arXiv*, 2024, preprint, arXiv:2410.20481, DOI: 10.48550/arXiv.2410.20481.
66 D. H. Case, J. E. Campbell, P. J. Bygrave and G. M. Day, Convergence Properties of Crystal Structure Prediction by Quasi-Random Sampling, *J. Chem. Theory Comput.*, 2016, **12**, 910–924.
67 S. Yang and G. M. Day, Exploration and Optimization in Crystal Structure Prediction: Combining Basin Hopping with Quasi-Random Sampling, *J. Chem. Theory Comput.*, 2021, **17**, 1988–1999.
68 P. W. V. Butler, R. Hafizi and G. M. Day, Machine-Learned Potentials by Active Learning from Organic Crystal Structure Prediction Landscapes, *J. Phys. Chem. A*, 2024, **128**, 945–957.
69 E. Dypvik Sødahl, J. Carrete, G. K. H. Madsen and K. Berland, Dynamical Disorder in the Mesophase Ferroelectric HdabcoClO$_4$: A Machine-Learned Force Field Study, *J. Phys. Chem. C*, 2025, **129**, 484–494.